In vivo histomorphological evaluation of geopolymer-carbonated apatite nanocomposites implanted on rabbit tibia at early bone healing

Dahlia Sutanto[1*], Mieke Hemiawati Satari[2], Bethy Suryawathy Hernowo[3], Bambang Pontjo Priosoeryanto[4], Rifki Septawendar[5], Lia Amelia Tresna Wulan Asri[6], Bambang Sunendar Purwasasmita[7]

[1]Department of Prosthodontics, Faculty of Dentistry Maranatha Christian University, Indonesia
[2]Department of Oral Biology, Faculty of Dentistry Universitas Padjadjaran, Indonesia
[3]Department of Pathology Anatomy, Faculty of Medicine Universitas Padjadjaran, Indonesia
[4]Department of Veterinary Clinic, Reproduction, and Pathology, Faculty of Veterinary Medicine IPB University, Indonesia
[5]Department of Advanced Ceramics, Glass, and Enamel, Center for Ceramics, Nanomaterials Research Group Ministry of Industry of The Republic of Indonesia, Indonesia
[6]Department of Materials Science and Engineering Research, Faculty of Mechanical and Aerospace Engineering Bandung Institute of Technology, Indonesia
[7]Department of Engineering Physics, Faculty of Industrial Technology Bandung Institute of Technology, Indonesia

ABSTRACT

Introduction: Dental implants have become a more desirable treatment for replacing missing teeth. The mechanical properties and biocompatibility of titanium and zirconia are excellent, but they are less bioactive. The chemical composition of the carbonate apatite is similar to enamel and dentin. Geopolymers are inorganic polymers, and they are similar to ceramics. They have excellent mechanical properties, bioactivity, biocompatibility. The purpose of this study was to assess histomorphological evaluation of geopolymer-carbonated apatite nanocomposites implanted on rabbit tibia at early bone healing in vivo. **Methods:** Geopolymer-CHA nanocomposites with a diameter of 3 mm and length of 6 mm was placed in the tibia of eight male New Zealand White rabbit whose body weight is 3 to 3.5 kg and six-month ages. Experimental subjects were randomly assigned to 2 groups for assessing the bone healing capability around samples to 14 and 28 days histomorphologically. Wilcoxon test was performed, and $p<0.05$ was considered significant, using Minitab software version 13. **Results:** Granulation tissue, woven, and lamellar bone was analysed. A reactive bone formation was revealed in the 14th day. Osteoblasts, osteoids, and osteocytes showed more mature and woven bone became denser on the 28th day. **Conclusion:** Geopolymer-CHA nanocomposites could be considered a candidate for dental implant material from this histomorphological evaluation.

Keywords: Histomorphological; geopolymer-CHA nanocomposites; dental implant; early bone healing.

p-ISSN: 1979-0201; e-ISSN: 2549-6212; Available from: http://jurnal.unpad.ac.id/pjd/article/view/2889
DOI: 10.24198/pjd.vol33no1.28899
Submission: Aug 01, 2020; Accepted: Mar 08, 2021; Published online: Mar 31, 2021.

**Corresponding author: Dahlia Sutanto, Department of Prosthodontics, Faculty of Dentistry Maranatha Christian University, Indonesia. 65, Jalan Surya Sumantri, Bandung, West Java, Indonesia, 40132. Phone: +62 812-2378-007; e-mail: dahlia.sutanto@dent.maranatha.edu*

INTRODUCTION

Implant supported denture are able to restore the masticatory function which affects the quality of life for edentulous patients. Bone healing event after implant placement is preceded by several stages until osseointegration occurs, which characterized by close contact between the implant surface and the surrounding bone.[1,2,3] Currently, titanium and zirconia are the most widely used as dental implant materials due to their biocompatibility and mechanical properties. However, there is disadvantage the elastic modulus of titanium (2222.7 ± 277.6 MPa) and zirconia (90 GPa) values are greater than enamel (1338.2 ± 307.9 MPa) and dentin (1653.7±277.9 MPa), less bioactive to stimulate osseointegration even the surface has been modified.[4,5,6,7,8,9,10]

Recently a large amount of research has been undertaken to develop materials that are suitable and adaptable to the biological environment to stimulate bone healing using inorganic materials such as calcium phosphate to simulate the chemical properties of bones and teeth. Geopolymers are inorganic materials that resemble ceramics, consisting of aluminosilicate precursors which are activated by a solution of alkaline activators such as sodium hydroxide and sodium silicate.[11]

Geopolymer have excellent mechanical properties including compressive strength, while from their biological properties they are bioactive, biocompatible, suitable to replace the hard tissue, and safe for the environment.[12,13,14,15,16] Combining geopolymers with other materials is a way of enhancing the excellent properties of geopolymers. According to Tippayasam et al.[17], the bioactive properties and biocompatibility of geopolymers are shown by their ability to increase bone-cell activity for new bone formation. Supported by Cataura et al.[18] that metakaolin-based geopolymer can be used as a hard tissue prosthesis.[12,17,18]

Carbonate and apatite are a mineral where apatite is calcium phosphate such as hydroxyapatite and fluorapatite. Carbonate apatite [$Ca_{10}(PO_4)_x(CO_3)_y(OH)_z$] is widely used as a biomaterial due to their similarity to bone and tooth composition, their ability to stimulate bone regeneration, allows bone growth onto and stimulates new bone formation. In vitro studies have demonstrated the role of calcium in the differentiation of preosteoblasts to osteoblasts.[12,19,20] According to Park et al.[21] calcium phosphate biomaterial is useful for bone repair because of their similarity to bone minerals and are biocompatible and osteoconductive.[21]

The process of healing bones after implant placement is repetitive process similar to bone development.[3,22,23] The first stage of the bone healing process is hematoma, followed by acute inflammation, granulation tissue, callus formation, and remodeling. The hematoma and inflammation stage lasted few days to a week after the fracture and is followed by the granulation tissue formation rich in mesenchymal cells which are the essential for bone formation and developing neovasculature which is the key factor for bone remodeling embedded in an unorganized extracellular collagen matrix in several days to a week after the injury, which as a starting point of bone healing.[24,25]

Subsequently, chondrocytes produce cartilage known as soft callus several weeks after the injury. At the same time, further bone formation occurs by intramembranous ossification especially in non-hypoxic areas. Mesenchymal cells differentiate into osteoblasts which in turn form woven bone. Blood vessel growth extending into the scaffold cartilage bridging the fracture gap, at the same time differentiating osteopregenitor cells into osteoblasts continues and followed by depositing woven bone on the cartilage scaffold, this stage lasts for several weeks or months and known as hard callus formation.

In the final stage, both immature woven bone and cartilage matrix are resorbed by osteoclasts, and the remodelling process begins and will last for several months to several years.[24] In this research, we was aimed to assess the histomorphological evaluation of geopolymer-carbonated apatite nanocomposites implanted on rabbit tibia at early bone healing in vivo.

METHODS

Sample preparation

Sodium hydrogen carbonate, calcium nitrate tetrahydrate, di-ammonium hydrogen phosphate, sodium hydroxide were obtained from Merck

and sodium silicate from Sigma-Aldrich. Kaolin was provided by the Center for Ceramics, Ministry of Industry of the Republic of Indonesia. Metakaolin was obtained by heating kaolin at 800^0 C. Carbonated apatite was synthesized by precipitation method. Ammonia solution was added drop-wise to 100 mL of calcium nitrate tetrahydrate 0.1 M and stirred until pH reached 9, followed by addition of 100 mL of diammonium hydrogen phosphate 0.06 M and 100 mL of sodium hydrogen carbonate 0.06 M. Ammonia solution was added to adjust pH to 9. Solution was stored at RT for 12 hours.

The suspension was centrifuged at 8000 rpm. The precipitate was separated and dried in an oven at 80°C for 30 min. The sample was then calcined at 700°C for 2 hours in air atmosphere. The final product was grinded using a mortar, resulting in a fine white powder. The geopolymer sample was prepared by mixing metakaolin with alkali activator containing sodium silicate and 12 M NaOH with w/w ratio of 2:1. The resulting paste-like mixture was poured into an acrylic mold and stored at the room temperature for 30 minute and then dried in the oven at 80° C for 20 hours and samples were cooled under the room temperature.

Biological characterisation

Material cytotoxicity testing was carried out using the trypan blue method to verify the morphology and viability of fibroblast cells. Sampels were tested in cylinder form with dimension of 3 mm and thickness of 6 mm, evaluated in duplicate. Samples were washed for 96 hours in demineralised water before used, which was changed every 24 hours.

Fibroblasts were cultured in medium RPMI 1640 (Gibco, USA) before placed in 6 wells, each containing 100% cells, followed by an incubation stage for 24 hours, 48 hours, and 72 hours at 37°C. After incubation, all culture media were aspirated into a centrifugal tube, each well was washed with 1 ml of saline phosphate buffer pH 7.4 (Gibco, USA) and collected into a centrifugal tube.

One ml of trypsin (Gibco, Denmark) was pipetted into each well, then incubated for 5 minutes. The incubated trypsin was aspirated and collected into each tube, cells were quantified with a hemocytometer (Neubauer Improved, Marienfeld, Germany) and cell morphology was analysed using a Motic Inverted Microscope (Olympus CK40) with a 10 MP resolution camera.

Physical characterisation

Material characterisation was carried out by Fourier-Transform Infrared Spectroscopy (FTIR) measurements recorded with KBr pellets on Prestige 21 Shimadzu to detect the differences in functional groups. The spectra was measured at a resolution 4 cm^{-1} with the number of scans 40 and at wavelength 4500–400 cm^{-1}. X-ray diffraction (XRD) analysis measured on Rigaku using Cu anode with wavelength of 1.5406 Å to detect the crystalline structure. The XRD measurement was collected at 2θ range of 15°–60°.

Animal

Eight male New Zealand rabbits, aged 6 month of age (weight 3.0-3.5 kg) were used in this research. During the experiment, each rabbit was kept in their own cage and fed once per day with standard laboratory diet and given tap water chow *ad libitum*. Animal selection, management, and surgery protocol had already gaining approval from Ethical Committee of IPB University with approval number of 151/KEH/SKE/VIII/2019. The study began after the animal had been adapted for 2 weeks.

Study design

The research was conducted on eight healthy male breeding New Zealand white rabbits, 6 month old, with the weight of 3.0-3.5 kg. Experimental subjects were randomly assigned to two groups for evaluating the early stage of bone healing capability around samples, one group consisted of 4 rabbits were evaluated for 14 days, and the other group consisted of 4 rabbits for 28 days.

Surgical procedure

The rabbit fur was shaved and the skin surface was cleaned with iodine solution in the tibia metaphysis prior to the surgery. Rabbits were anaesthetised with combination of 10 mg/kg of ketamin hydrochloride (Pharmamadix Corp, Peru) and 3 mg/kg of xylazine hydrochloride (Interchemie werken "De Adelaar" BV, Venray, Holland) intramuscular. Additionally, a local anaesthetic of 0.5 ml/adrenaline of lidocaine (PT.

Bernofarm Pharmaceutical Company, Jakarta) was applied subcutaneously. During surgery, all rabbits were infused with lactated Ringer's solution. After the skin and subcutaneous tissues incision were performed, the muscles and periosteum were dissected to expose the bone surface of tibia metaphysis. Bone defects with the width of 3 mm and the depth of 6 mm were performed using the low speed drill with continuous irrigation.[26]

Samples with the diameter of 3 mm and length of 6 mm were thoroughly rinsed with sterile saline before insertion and positioned in the tibia metaphysis as showed in Figure 1A. The wound was closed with a resorbable 3.0 polyglygolic acid coated white sutures (Surgifit®, Busan, Korea). Afterwards, the samples were allowed to be self-healed under the skin as showed in Figure 1B. 1.1 mg/kg of Analgesic Fortis® (Dong Bang Co, Ltd, GYeonggi-do, Korea) and 10 mg/kg of Genta-100® (Interchemie werken "De Adelaar" BV, Venray, Holland) were administered via intramuscular injection after surgery and following 3 days after surgery, topical application of nebacetine ointment (Pharos, Jakarta) in the wound area until healed.

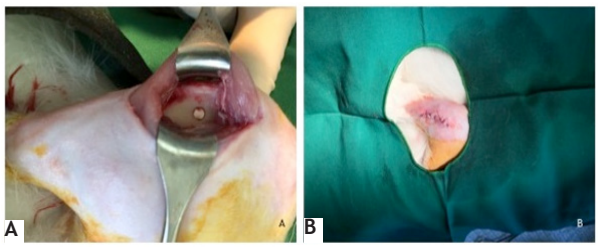

Figure 1. (A). Sample with 3 mm in diameter and 6 mm of length was positioned in tibia metaphisis; (B). Primary wound closure and sample was left to heal

Animal sacrification and retrieval of specimen

The rabbits were euthanised used overdose of penthobarbital sodium phenytoin 0.5 cc/kg body weight intravenous after 14 days and 28 days postoperative. Tibia was dissected and a segment of metaphysis about 2.0 cm in length comprising the sample was obtained for histological study. All dissected bone segments were fixed in 10% neutral-buffered formalin solution for 24 hours.

Histological preparation

After 24 hours of fixation and additional 96 hours of decalcification with a commercial EDTA-hydrochloric acid mixture (Surgipath Decalcifier II, Leica Biosystem, USA). The bone segment was cut longitudinally with a sample plane, dehydrated used ascending grades of 70%, 80%, 90%, and 96% alcohol, followed by absolute ethanol 1 and absolute ethanol 2 for two hours each concentration. Afterwards, the segment were dipped in xylol 1, xylol 2, and xylol 3 and followed by paraffin infiltration (Thermo Scientific Histoplast, Cheshire, WA7 1TA, UK). The sample was cut to a thickness of 5 micrometers using microtome, and placed on a slide coated with poly-L-lysine (Sigma– Aldrich, Gillingham, UK).

The slide was placed on a hotplate at 56-60^0 C for 10 minutes, then stored in an incubator at 38^0-40^0 C for a night. After incubated, all slides were deparafinised with xylol, followed by rehydration with xylene for 10 minutes then tapped under running water for 5 minutes. Samples were stained with Haematoxylin and Eosin (H&E) to identify areas of new bone formation.

Statistical analysis

Statistical analysis was performed on the percentage of granulation tissue, woven bone, and lamellar bone, using Wilcoxon test, with $p<0.05$ considered as statistically significant. Statistical tests were conducted with Minitab version 13 software.

RESULTS

Characteristic of carbonate bands observed at 1415, 1462, and 875 cm^{-1}, which confirmed the formation of carbonated apatite type A and B as shown by the peak at 1417 cm^{-1}, 1412 cm^{-1} and type B carbonates at the peak 1415 cm^{-1} (Figure 2). The XRD pattern showed that the sample consisted of pure hydroxyapatite phase according to PDF was 2.841998. The hydroxyl apatite in the CHA was shown by three main peak of the hydroxyapatite phase angles 2θ of 31.80°, 32.23°, and 32.96°, corresponded to the (121), (112), and (300) crystal plane of the hexagonal structures of hydroxyl apatite (Figure 3).

In vitro fibroblast cell viability test showed that the number of living cells >80%, with no morphological changes, and the samples were apparently biocompatible. After incubation for 72 hours, the percentage of living cells was 94.2% as showed in Figure 4 and Figure 5.

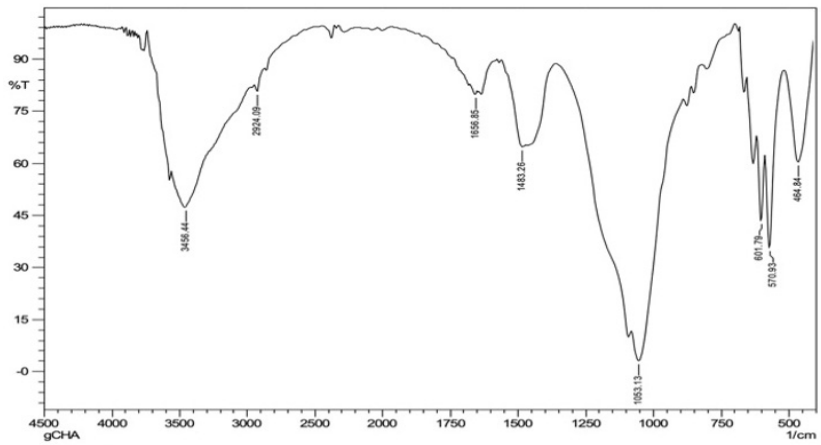

Figure 2. FTIR spectra of geopolymer-carbonated apatite nanocomposites

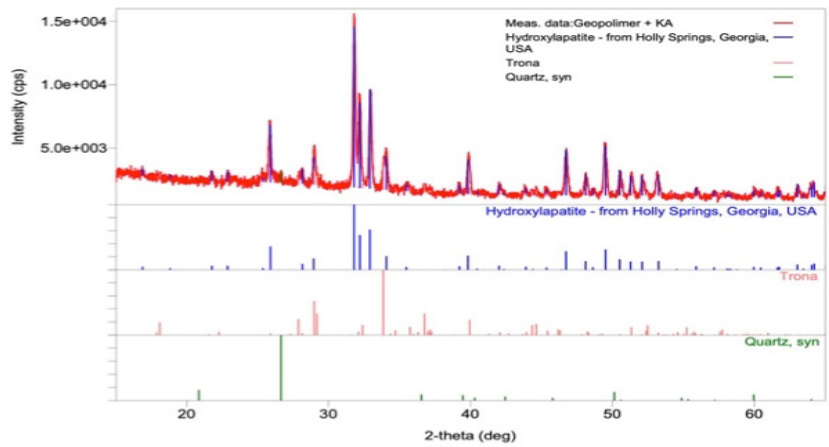

Figure 3. XRD pattern of geopolymer-carbonated apatite nanocomposites

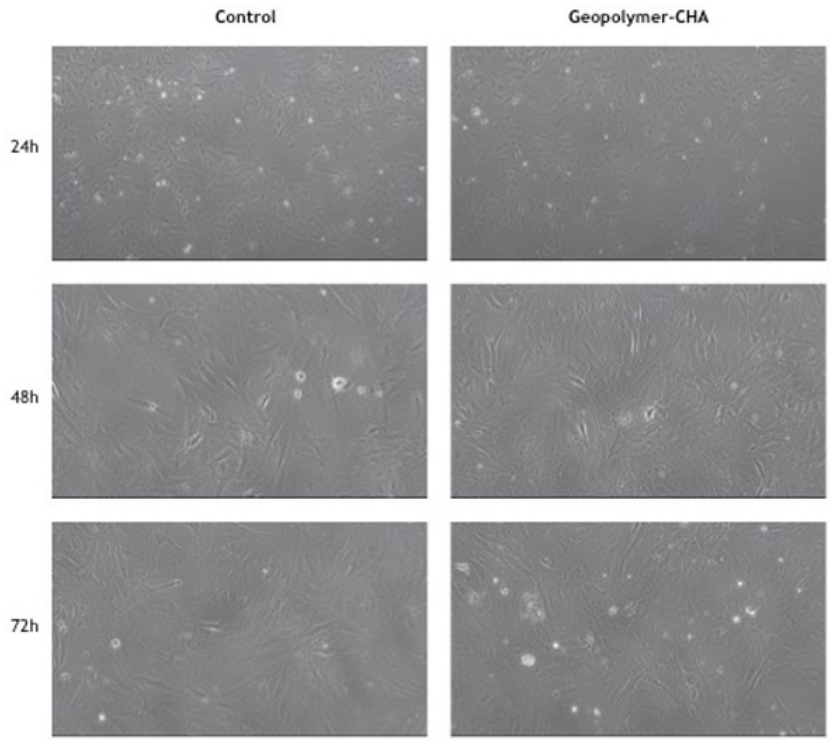

Figure 4. Microscope images of mouse embryonic fibroblasts after 24, 48 and 72h incubation on control group and geopolymer-CHA nanocomposites. The bar denotes 50 µm

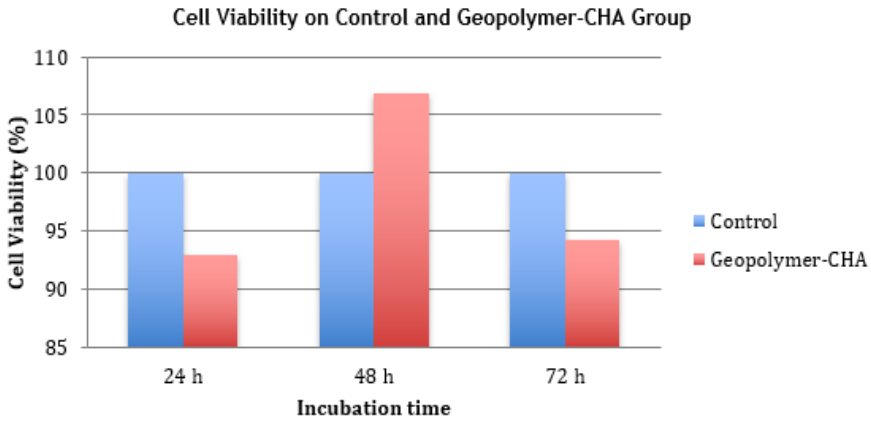

Figure.5 Fibroblasts cell viability on control and geopolymer-CHA groups after 24, 48 and 72 hours of incubation

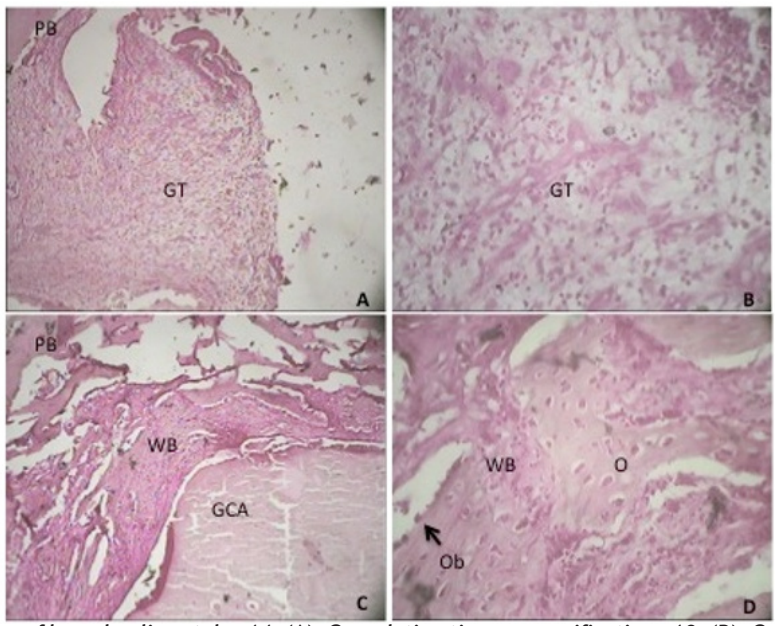

Figure 6.Histological view of bone healing at day 14: (A). Granulation tissue, magnification x10; (B). Granulation tissue consist of vascular proliferation, fibroblasts, and inflammation cells, magnification x40; (C). Parent bone (PB), woven bone (WB) - reactive bone formation, geopolymer-carbonated apatite (GCA), magnification x10; (D). Woven bone (WB), osteoids (O), Osteoblasts (Ob), original magnification x40

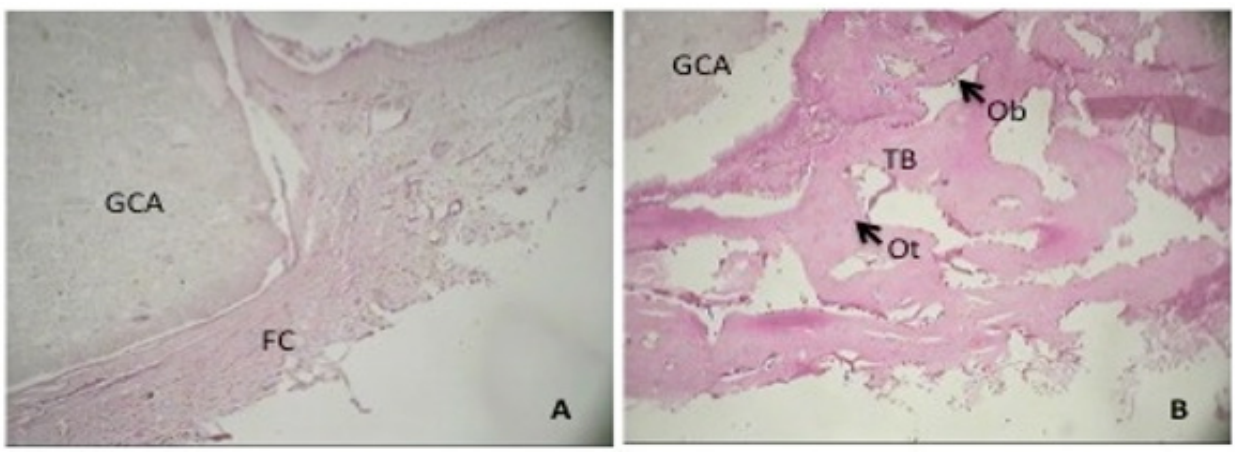

Figure 7. Histological view of bone healing at day 28: (A). Dense fibro collagen adjacent geopolymer-carbonated apatite (GCA), magnification x10; (B). Parent trabecular bone (TB) moved toward geopolymer-carbonated apatite (GCA), Osteoblasts (Ob), Osteocytes (Ot), magnification x40

Table 1. Granulation tissue, woven bone, lamellar bone at 14 and 28 days

Variable	Mean	SE Mean	StDev	Minimum	Q1	Median	Q3	Maximum
Granulation	0.875	0.125	0.354	0.000	1.000	1.000	1.000	1.000
Woven bone	0.875	0.125	0.354	0.000	1.000	1.000	1.000	1.000
Lamellar bone	0.875	0.125	0.354	0.000	0.000	0.000	0.000	1.000

Table 2. Wilcoxon signed rank test of granulation tissue , woven bone, lamellar bone at 14 and 28 days

	N	N for Test	Wilcoxon Statistic	P	Estimated median
Granulation	8	8	31.5	0.069	1
Woven bone	8	8	31.5	0.069	1
Lamellar bone	8	8	4.5	0.069	0

Histological examination 14 days postoperative

In 14 days postoperative, there were no inflammatory infiltrate, bone resorption, likewise allergic reactions, abcesses, and infections during the observation period. Our histological results showed a gap between the sample and the surrounding bone has been filled with granulation tissue containing mesenchymal cells, development of new blood vessels, and fibroblasts in an organised extracellular collagen matrix as showed in Figure 6.

Histological examination 28 days postoperative

In 28 days postoperative, dense fibro collagen connective tissue that which is the forerunner to cartilage was observed between the samples surface and adjacent bone as showed in Figure 7.

Different cell locations and shapes could be identified through Haematoxylin and Eosin (H&E) staining. Osteocytes and osteoblasts were present in hard tissue components while fibroblasts were presented in the connective tissue. Wilcoxon rank test showed no significant different between the granulation tissue, woven bone, and lamellar bone on the 14th and 28th days with the p-value of 0.069, as presented in Table 1 and Table 2.

DISCUSSION

Bone healing after implantation is a fracture healing process that recapitulates bone development. The first cascade of fracture healing is hematoma formation followed by acute inflammation, granulation tissue, callus formation, and remodeling. Several days to week after implantation, the inflammatory stage is replaced by granulation tissue which is the key factor for bone formation.[24] On the tissue level of bone formation is characterized by the initial deposition of collagen matrix in a irregular oriented pattern which referred as woven bone.

In this study, histomorphological evaluation showed loosen woven bone with immature osteoids in its matrix formed adjacent the sample area which showed there was a reactive bone formation, as demonstrated in Figure 6, Futhermore, immature osteoblasts were observed to be arranged around the sample area, and osteocytes were embedded with the newly formed bone on the 14th day.

On the 28th day, the woven bone was showed to be denser with mature osteoids in the matrix, osteoblasts and osteocytes were more mature than on the 14th day and scattered around the sample area irregularly. These results showed that geopolymer-carbonated apatite nanocomposites had a potential of osteoconductivity and bioactivity properties by initiating and supporting osteogenesis in the initial healing cascade.

These observation results were consistent with Loi et al.[24], which stated that the hematoma and inflammation stages will end within a few days to one week after the bone fracture and will be replaced by granulation tissue formation. The proliferation of blood vessels will result a better blood supply which allows the recruitment of mesenchymal cells which then differentiate into osteoprogenitor cells, osteoblasts, and eventually lay out woven bone contained of immature osteoids, which indicated there was reactive bone formation as showed in Figure 6. This condition was also consistent with the research conducted by Chug et al.[27], which suggested that

the formation of osteoid-rich woven bone signifies the beginning of new bone formation.

Osteoconductivity refers to the ability of a material to allow unimpeded bone growth onto or throughout.[28] While bioactivity refers to the ability of a material to develop a direct, adherent, and strong bonding with the bone tissue.[29] This result was in the a agreement according to Tippayasam et al.[17] reported that the bioactive properties and biocompatibility of geopolymers were shown by their ability to increase bone-cell activity for new bone formation.[17] Cataura et al.[18] stated that metakaolin-based geopolymer could be used as a hard tissue.[18]

Ramazanoglu et al.[30] classified ossification into three groups, namely biotolerant, where new bone formation occurs around the bone and migrates towards the implant surface (distance osteogenesis), bioinert that was characterised by the formation of new bone directly on the implant surface (contact osteogenesis), bioreactive which was the implant allowed new bone formation actively on the implant itself.[30] Our result indicated that geopolymer-carbonated apatite nanocomposites had the potential of biotolerant and bioreactive properties characterised by distance osteogenesis and samples allowed new bone formation as showed in Figure 7. In this study, analysis was carried out on granulation tissue, woven bone, and lamellar bone with consideration of granulation tissue contains many mesenchymal cells and neovascular.[24] Mesenchymal cells will differentiate into osteoprogenitor and osteoblast cells which are supported by angiogenesis. The presence of granulation tissue indicates an early stage of new bone formation.[25] Osteoprogenitor cells would differentiate into osteoblasts that directly laid out woven bone, indicated the development of cortical bone, followed by collagen matrix deposition in regular and parallel orientation known as lamellar bone.[31]

Although statistically showed the presence of no significant different in the percentage between granulation tissue, woven bone, and lamellar bone on the 14th and 28th day, however histological observations showed the different woven bone densities between days 14 and 28, as well as the level of maturity of bone cells which showed more mature on the 28th day. Considering implant is an artificial root substitute that will be close contact with the surrounding bone, the mechanical properties of dental implant material should not exceed the mechanical properties of tooth structure to preserve the parent bone bed.

In this study, it was found that geopolymer-CHA nanocomposites reached the range of dentin hardness value, tensile strength and compressive strength reached the range of enamel, while modulus elasticity reached the range of enamel and almost reached dentin. In vitro biocompatibility test showed sample was not toxic, in vivo histomorphological evaluation demonstrated good response of bone cell on the sample surface, indicated by the initial bone healing which characterised by formation of granulation tissue, woven bone rich in osteoid and surrounded by osteoblast around samples. From the mechanical and biological properties point of view, our result showed that geopolymer-carbonated apatite nanocomposites was potential candidates as dental implant materials.

Limitations of this study include the small number of rabbits in each group and the short time limit of observation from operation and euthanized.

CONCLUSION

From this histomorphological evaluation, Geopolymer-CHA nanocomposites could be considered as a candidate for dental implant material

REFERENCES

1. Carlo S Di, Angelis F De, Brauner E, Rosella D, Papi P, Pompa G, et al. Histological and immunohistochemical evaluation of mandibular bone tissue regeneration. Int J Immunopathol Pharmacol. 2018;32:1–8. DOI: 10.1177/2058738418798249
2. Villar CC, Huynh-ba GUY, Mills MP, Cochran DL. Wound healing around dental implants. Endodontic Topics. 2012;25:44–62. DOI: 10.1111/etp.12018.
3. Colombo JS, Satoshi S, Okazaki J, Crean S, Sloan AJ, Waddington RJ. In vivo monitoring of the bone healing process around different titanium alloy implant surfaces placed into fresh extraction sockets. J Dent. 2012;40(4):338–46.

4. Almola BH, Al-ghaban N, Taher A. Deposition at amelogenin coated Ti implant surface. Smile Dent.J. 2016;9(1):12-17. DOI: 10.1016/j.jdent.2012.01.010
5. Saini M, Singh Y,Arora P, Arora V JK. Implant biomaterial: A comprehensive review. World J Clin Cases. 2015;3(1):52–7.DOI: 10.12998/wjcc.v3.i1.52
6. Shi J, Li Y, Gu Y, Qiao S, Zhang X, Lai H. Effect of titanium implants with strontium incorporation on bone apposition in animal models : A systematic review and meta-analysis. Scientific Reports. 2017; (11):1–10. DOI: 10.1038/s41598-017-15488-1
7. Apratim A, Eachempati P, Salian KKK, Singh V, Chhabra S, Shah S. Zirconia in dental implantology: A review. J Int Soc Prev Community Dent. 2015;5(3):147-56.DOI: 10.4012/dmj.2019-172
8. Chun KJ, Lee JY. Comparative study of mechanical properties of dental restorative materials and dental hard tissues in compressive loads. J. Dent. Biomech. 2014;(5):1–6. DOI: 10.1177/1758736014555246
9. Cui WF, Liu N, Qin GW. Microstructures, mechanical properties and corrosion resistance of the Zr e x Ti (Ag) alloys for dental implant application. Mater. Chem. Phys. 2016; 6(8): 2569-2612 DOI: 10.1016/j.bioactmat.2021.01.030
10. Zhang BG, Myers DE, Wallace GG, Brandt M, Choong PF. Bioactive coatings for orthopaedic implants-recent trends in development of implant coatings. Int J Mol Sci. 2014; 15(7): 11878-921. DOI: 10.3390/ijms150711878
11. Cataura M, Bollino F, Papale F, Lamanna G. Investigation of the sample preparation and curing treatment effects on mechanical properties and bioactivity of silica rich metakaolin geopolymer. Mater Sci Eng C Mater Biol Appl. 2014; 36: 20-4. DOI: 10.1016/j.msec.2013.11.026
12. Sauffi AS, Ibrahim WMW, Mustafa M, Abdulla MMAB, Ahmad R, Zaidi FA,et al. A review of carbonate minerals as an additive to geopolymer materials. Mater Sci Eng. 2019; 551:1-5. DOI: 10.1088/1757-899X/551/1/012084
13. Chen L, Wang Z, Wang Y, Feng J. Preparation and Properties of Alkali Activated Metakaolin-Based Geopolymer. Materials (Basel). 2016; 9(9): 767. DOI: 10.3390/ma9090767
14. Rovnanik P. Effect of curing temperature on the development of hard structure of metakaolin- based geopolymer. Constr Build Mater. 2014; 24(7): 1176–83. DOI: 10.1016/j.phpro.2011.11.048
15. Herwani H, Pane I, Imran I, Budiono B. Compressive strength of fly ash-based geopolymer concrete with a variable of sodium hydroxide (NaOH) solution molarity. MATEC Web Conf. 2018; 147:1-5. DOI: 10.1002/fam.2240
16. Blaszczynski TZ, Krol MR. Alkaline activator impact on the geopolymer binders. Mater Sci Eng. 2017; 245: 1–11.DOI: 10.1007/s43207-020-00060-x
17. Tippayasam C, Sutikulsombat S, Kamseu E, Rosa R, Thavorniti P, Chindaprasirt P, Leonelli C, Hennes G, Chaysuwan D. In vitro surface reaction in SBF of a non-crystalline aluminosilicate (geopolymer) material. Aust Ceram Soc. 2018;(6):1–7. DOI: 10.1007/s41779-018-0205-4
18. Cataura M, Bollino F, Kansal I, Kamseu E, Lancellotti I, Leonelli C. Mechanical and biological characterization of geopolymers for potential application as biomaterials. Azo J Mater. 2012; (5):1–15. DOI: 10.2240/azojomo0322
19. Eliaz N, Metoki N. Calcium phosphate bioceramics : A review of their history, structure, properties, coating technologies and biomedical applications. Materials. 2017; (3):1-104. DOI: 10.3390/ma10040334
20. Barradas AMC, Fernandes HAM, Groen N, Chai YC, Schrooten J, Peppel JVD, et al. A calcium-induced signaling cascade leading to osteogenic differentiation of human bone marrow-derived mesenchymal stromal cells. Biomaterials. 2012; 33(1): 1-11. DOI: 10.1016/j.biomaterials.2012.01.020
21. Park JH, Lee EJ, Knowles JC, Kim HW (2014). Preparation of in situ hardening composite microcarriers: calcium phosphate cement combined with alginate for bone regeneration. J Biomater Appl.2014;28(7):1079-1084. DOI: 10.1177/0885328213496486
22. Marsell R, Einhorn TA, The biology of fracture healing. NIH Public Access. 2012; 42(6): 551–5. DOI: 10.1016/j.injury.2011.03.031

23. Terheyden H, Lang NP. Bierbaum S, Stadlinger B. Osseointegration – communication of cells. Clin Oral Impl Res.2011; 23: 1127–35. DOI: 10.1111/j.1600-0501.2011.02327.x
24. Loi F, Córdova LA, Pajarinen J, Lin TH, Yao Z, Goodman SB. Inflammation, fracture and bone repair. Bone. 2016; 86(3): 119–30. DOI: 10.1016/j.bone.2016.02.020
25. Ghiasi MS, Chen J, Vaziri A, Rodriguez EK, Nazarian A. Bone fracture healing in mechanobiological modeling : A review of principles and methods. Bone Reports. 2017; 6(3): 87–100. DOI: 10.1016/j.bonr.2017.03.002
26. Hoffmann O, Angelov N, Zafiropoulos GG, Andreana S. Osseointegration of zirconia implants with different surface characteristics: an evaluation in rabbits. Int J Oral Maxillofac Implants. 2012; 27(2): 352-8.
27. Chug A, Shukla S, Mahesh L, Jadwani S. Osseointegration-molecular events at the bone-implant interface: A review. J Oral Maxillofac Surgery Med Pathol. 2013; 25(2): 1–4. DOI: 10.1016/j.ajoms.2012.01.008
28. Bose S, Fielding G, Tarafder S, Bandyopadhyay A. Understanding of dopant-induced osteogenesis and angiogenesis in calcium phosphate ceramics. Trends Biotechnol. 2013; 31(10): 594-605. DOI: 10.1016/j.tibtech.2013.06.005
29. Muddugangadhar BC, Amarnath GS, Tripathi S, Dikshit S, Divya MS. Biomaterials for dental implants: An overview. J. Clin.Oral Implants Res.2011; 2(1): 13-24. DOI: 10.5005/jp-journals-10012-1030
30. Ramazanoglu M, Oshida Y. Osseointegration and bioscience of implant surface-current concepts at bone-implant interface. In: Implant Dentistry - A Rapidly Evolving Practice. London: InTech Open; 2020. p. 57–82.
31. Shapiro F, Wu JY. Woven bone overview : Structural classification based on its integral role in developmental, repair and pathological bone formation throughout vertebrate groups. Eur Cells Mater. 2019; 38: 137–67. DOI: 10.22203/eCM.v038a11